I. E. T. Iben

Head reliability of AMR sensors based on thermal stress tests

Tape storage drives use robust shielded anisotropic magnetoresistive (AMR) read sensors. Under normal operating conditions, changes in sensor properties are undetectable. To estimate end-of-life conditions, sensors are exposed to elevated temperatures, and changes in relevant physical parameters are measured. Then, using thermodynamic models, these measurements are extrapolated to normal operating conditions. Thermal stress experiments using elevated electrical currents for heating were conducted on AMR read sensors designed for use up to about 200 Mb/in.² in tape storage drives. Physical parameters that are relevant to tape-drive function include stripe resistance, AMR amplitudes and asymmetries, and stripe and shield oxidation. Changes in these parameters were measured as functions of time and temperature. The experimental results were fit to thermodynamic models, which were then used to extrapolate the observed changes to normal operating temperatures and extended times. The data shows that, at the lowest temperatures, the important processes are stripe oxidation and annealing-induced changes in magnetic characteristics. For the materials studied, the projected timeto-failure for use in a drive is greater than ten years.

Introduction

Modern tape storage drives use sensors to read magnetic signals (transitions) written on tape. Anisotropic magnetoresistive (AMR) read sensors are primarily used in this application [1–4]. The resistance of an AMR material is larger when the direction of current flow and the direction of magnetization are parallel (0°) than when they are perpendicular to one another (90°). The maximum AMR amplitude is defined as the fractional change in resistivity between 0° and 90° states. Thus, magnetic transitions written on tape are detected by an AMR stripe as a resistance change in response to a rotation in the direction of stripe magnetization. To maintain linear response, the stripe magnetization is aligned at an angle of $\sim 45^{\circ}$ with respect to the direction of current flow, and the fields sensed from the tape are designed to be a fraction of the magnitude required to rotate the stripe magnetization to an angle of 0° or 90°.

An important consideration in designing a read sensor and its operating parameters is drive reliability. One critical parameter for drive reliability is the signal amplitude. Because it is the nature of the metal particulate tape medium to have particle density distributions, tape drives are designed to accommodate relatively large fluctuations in amplitude. Furthermore, because the noise in tape drives is dominated by noise originating from inhomogeneity in the magnetic coating of the tape, a larger range in amplitudes must be tolerated than can be tolerated in hard disk drives (HDDs), where electronics noise is equal to or greater than the noise from the HDD medium [3, 4]. Catastrophic failure is often preceded by a decrease in performance as quantified by the bits per error rate (BER). In modern high-quality tape-drive systems, BER values of 10⁵ or better are achieved. Changes in the sensor response over time can result in degraded performance with lower BER values,

Copyright 2003 by International Business Machines Corporation. Copying in printed form for private use is permitted without payment of royalty provided that (1) each reproduction is done without alteration and (2) the *Journal* reference and IBM copyright notice are included on the first page. The title and abstract, but no other portions, of this paper may be copied or distributed royalty free without further permission by computer-based and other information-service systems. Permission to *republish* any other portion of this paper must be obtained from the Editor.

0018-8646/03/\$5.00 © 2003 IBM

and ultimately in failure. To achieve high BERs in addition to sufficient AMR amplitude, it is necessary to minimize signal distortion from nonlinear signal response or magnetic density-dependent signals.

While published papers have addressed reliability associated with large resistance changes or drops in amplitude [5-9], few, if any, have directly addressed changes in signal distortion or magnetic-transition densitydependent responses (Wallace spacing losses) [10]. Signal distortion arises from a nonlinear response to magnetic field magnitude or direction. The nonlinear response of a read sensor is determined by measuring the difference in the absolute value of the AMR resistance change from oppositely oriented magnetic fields, which respectively rotate the stripe magnetization toward 0° or 90° with respect to the direction of current flow (asymmetry). With the transition from peak detect to partial response maximum likelihood (PRML) channels [3, 4, 11], drives are becoming more sensitive to signal distortion effects. Magnetic density-dependent responses lead to an exponential decrease in signal amplitude with an increase in the longitudinal density of magnetic transitions written on the tape due to interference [3, 4, 10]. As the longitudinal density increases, magnetic density-dependent losses become important for head-tape spacings of several tens of nanometers. In this paper, the time and temperature dependence of the resistance, amplitude, and asymmetry of AMR sensors are measured and fit to thermodynamic models. Oxidation of the stripe and shields is also measured, and the effect of oxidation on the magnetic density-dependent response is analyzed. Although readers that are actually used in drives are more complicated to understand than are sheets of single-material alloys, the former are studied in order to understand the complete system. The data is then used to determine the time-to-failure (TTF) under use conditions in a drive.

Experimental details

Materials

All sensors used in this study were shielded AMR sensors built for use in high-density magnetic tape storage applications for magnetic transitions of the order of 4×10^6 to 7×10^6 flux reversals per meter (frpm). A schematic diagram of a shielded sensor is shown in Figure 1 of [12] (this issue). The AMR stripes used in this study are multilayered sheets of metallic alloys that include a Co alloy soft adjacent layer (SAL), a Ta spacer, an 81 Permalloy (Ni:Fe, 81:19) AMR stripe, and a Ta cap. The AMR stripe material is chosen to be 81 Permalloy because its coefficient of magnetostriction (deformation when in a magnetic field) is close to zero [13, 14]. All of the metals

in the stripe are ion-beam deposited. On either end of the sheet is a permanent magnet, termed *hard-bias*. The hard-bias magnets and SAL are present for self biasing of the magnetization [3, 4].

The AMR stripe is separated from magnetically soft shields S1 and S2 by alumina (Al₂O₂) with a total gap of either 0.37 or 0.5 μ m. Shield S1 is 1.8- μ m-thick annealed Sendust (Fe:Si:Al, 83:12:5). Shield S2 is 3-μm-thick 81 Permalloy. The stripes are rectangular, with a track width (W) of 12.6 μ m along the x-axis and a stripe height (H) ranging from 1.5 to 3.0 μ m along the z-axis. The plane of the stripe (xz-plane) is perpendicular to the plane of the air-bearing surface (ABS) (xy-plane). The track width defines the read width of magnetic transitions read from tape. The thickness of the AMR stripe layer (t_{mr}) is either 30.0 or 40.0 nm, with respective SAL thicknesses (t_{SAL}) of 24.0 and 28.0 nm. The thickness of the Ta spacer and cap layers are 6.0 and 3.0 nm, respectively. The stripe resistance ($R_{\rm sheet}$) is 6.2 Ω/\Box and 4.6 Ω/\Box for $t_{\rm mr}$ values of 30.0 and 40.0 nm, respectively. To stabilize the sensors during the wafer processing, the hard-bias permanent magnets are created on either end of the sheet resistor along the length of the stripe height by deposition of magnetic material. These hard-bias magnets are later aligned in a magnetic field. The combined resistance of the internal leads and the hard bias (R_{lhb}) is around 8 Ω . The stripe thermal coefficient of resistance $[\alpha_{\rm mr} = (dR_{\rm mr}/dT)/R_{\rm mr}]$ is 0.0025° C⁻¹.

Joule heating

Because of joule heating, sensors operate at elevated temperatures [12]. The temperature distribution within a powered sensor and the surrounding shields results in stresses that are not present in uniform oven-heating experiments [15]. Furthermore, the distribution of temperatures in the stripe and shields results in oxidation profiles that are not reproduced in an oven experiment. Given the high current densities of AMR stripes used for reading recorded magnetic signals, another potential source of stripe degradation not present in oven experiments is electromigration [7, 8, 16, 17]. For these reasons, joule heating was chosen as the method of stresstesting the heads. Because the thickness and electrical conductivity of the leads are both much larger than those of the stripe, joule heating of the leads is minimal compared with that of the sheet. The resistance of the stripe (R_{mr}) is determined by subtracting the combined resistance of the leads and of the hard-bias magnets (R_{lbb}) from the total resistance (R_{total}) :

$$R_{\rm mr} = R_{\rm total} - R_{\rm lhb} = R_{\rm sheet} W/H. \tag{1}$$

Owing to manufacturing tolerances, W is defined extremely accurately at fabrication, but H [which is

calculated from Equation (1)] varies widely among devices. The temperature $(T_{\rm mr})$ of a stripe can be calculated from the measured stripe resistance $[R_{\rm mr}(T_{\rm mr})]$ using

$$R_{\rm mr}(T_{\rm mr}) = R(T_{\rm a})[1 + \alpha_{\rm mr}(T_{\rm mr} - T_{\rm a})], \tag{2}$$

where $T_{\rm a}$ (= 25°C) is an arbitrarily chosen reference temperature.

During joule heating, the temperature rise of an AMR stripe above the ambient substrate (material in which the stripe is embedded) temperature $T_{\rm s}$ ($\Delta T_{\rm mr}$) is proportional to the power ($P_{\rm mr}$) in the AMR stripe. Thus, $T_{\rm mr}$ is given by

$$T_{\rm mr} = T_{\rm s} + \Delta T_{\rm mr} = T_{\rm s} + P_{\rm mr}/k_{\rm mr} = T_{\rm s} + R_{\rm mr}(T_{\rm mr})I_{\rm mr}^2/k_{\rm mr},$$
 (3)

where $I_{\rm mr}$ is the current in the AMR stripe and $k_{\rm mr}$ is the thermal conductance of the sensor. The quantity $k_{\rm mr}$ is a measured parameter that is a function of the sensor dimensions and material thermal conductivities, particularly of the gap alumina and shield materials [12]. Although the resistance of the stripe can change irreversibly owing to various physical processes such as material annealing or interdiffusion of metals, the solubility of the stripe metals in alumina is negligible, so little, if any, metal should diffuse into the gap alumina. Thus, $k_{\rm mr}$ is measured prior to the degradation experiments and is assumed not to change during the experiment.

Thermal stress experiments

In these experiments, current is applied to a group of elements simultaneously. Additional elements embedded within the same substrate are not powered and are used to determine T_s using Equation (2) with $T_{mr} = T_s$. Each powered element is cycled between a low and a high power level, which is different for each element. The high power levels are chosen to achieve a range of temperatures appropriate for observing changes in the magnetic or electrical properties of the stripe or oxidation of the metals exposed to air at the ABS. The resistance of and current flow through each stripe is measured at regular intervals during the high-power portion of the cycles to determine the hot-stripe temperature using Equation (3). Power in the elements during the highpower intervals of these experiments also results in a temperature rise of the substrate above the ambient air temperature [14] to values between 40°C and 70°C. The time dependence (t) of the change in stripe resistance is determined by measuring the resistance at the end of each cold cycle $[R_{mr0}(t, T_{mr})]$, when the stripe has reached a stable temperature. t is the integrated time that a sensor has been exposed to the temperature $T_{\rm mr}$. The low-power levels are chosen so as to minimize joule heating and to accurately determine R_{mr0} .

Magnetic changes: Asymmetry and amplitude

To determine the time dependence of the magnetic properties of the sensors, the sensors were removed from the thermal stress apparatus after being exposed to elevated joule-heating temperatures for different lengths of time, and the AMR response was measured. The quantities measured were the magnetic amplitude (Amp) and asymmetry (Asy), as defined by Equations (4a) and (4b), respectively:

$$Amp = (R_{\rm p} + R_{\rm n}) \tag{4a}$$

and

$$Asy = 100\% (R_{p} - R_{p})/(R_{p} + R_{p}), \tag{4b}$$

where $R_{\rm p}$ and $R_{\rm n}$ are the absolute values of the change in stripe resistance at a fixed $I_{\rm mr}$ resulting from the AMR resistance change of the stripe in response to magnetic fields of the same magnitude oriented parallel to the stripe height and in opposite directions ($\pm z$ axis).

One method for measuring the amplitude and asymmetry of the sensor is to read the magnetic transitions recorded on magnetic tape. In these experiments, the highest longitudinal density used is 3.66×10^6 frpm. Another instrument used to measure amplitude and asymmetry is a quasi-static tester, which applies a homogeneous magnetic field perpendicular to the ABS along the stripe height direction. One quasi-static tester applies a uniform magnetic field to the sensors of 0 and ±120 Oe. A field of 120 Oe was chosen to achieve quasi-static amplitudes of the same approximate level as measured when reading signals from a magnetic tape with a longitudinal density of 3.66×10^6 frpm. At each field, 500 measurements are made, and the averages recorded. The signals are measured as voltages given by the product of $I_{\rm mr}$ and $R_{\rm mr}$. Values for $I_{\rm mr}$ of 12 and 14 mA are used for sensors with t_{mr} of 30.0 and 40.0 nm, respectively. A second quasi-static tester is used to measure transfer curves of AMR resistance as a function of a magnetic field between +600 and -600 Oe. The field is first stepped up from 0 to +600 Oe, then stepped down from 600 to -600 Oe, and finally stepped back up from -600 to 0 Oe, all in increments of 1 Oe. Because the studied sensors that use the high fields all have $t_{\rm mr}$ values of 40.0 nm, $I_{\rm mr}$ is chosen as 14 mA.

Oxidation

Thermally assisted oxidation of the sensor materials is achieved by joule heating in the same manner as in the thermal stress experiments to determine thermally induced electrical and magnetic changes. The growth of oxidation above the ABS of the sensors and shields is determined by atomic-force-microscope (AFM) measurements.¹

¹ Nanoscope IIIa from Digital Instruments, Santa Barbara, CA

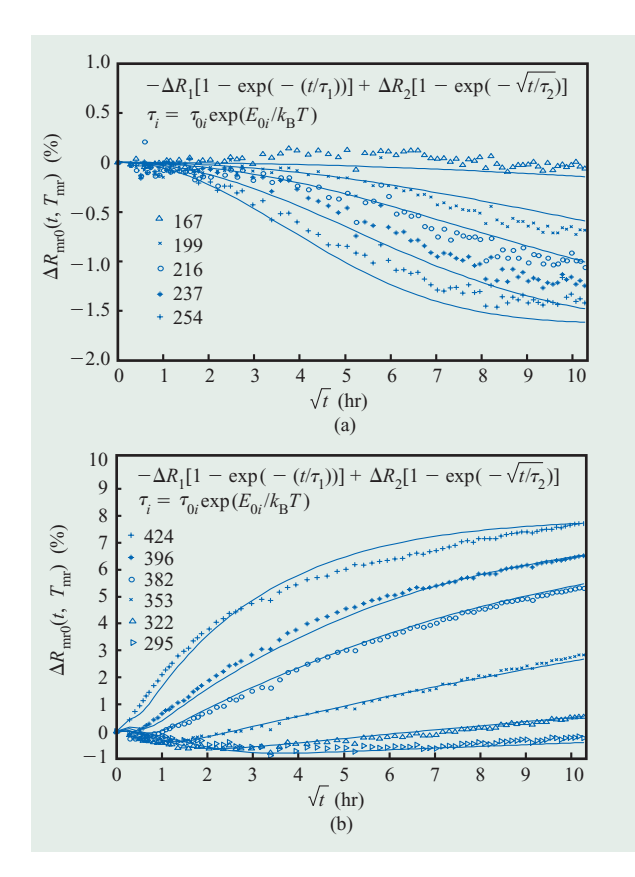


Figure ⁻

Plot of the fractional resistance change at ~21°C as a function of \sqrt{t} for AMR stripes that have been heated to (a) $167^{\circ}\text{C}-254^{\circ}\text{C}$ and (b) $295^{\circ}\text{C}-424^{\circ}\text{C}$. The fits are described in the text. The sensor t_{mr} , gap, and H are 40.0 nm, $0.5\,\mu\text{m}$, and $2.4\,\mu\text{m}$, respectively.

Results and analysis

Thermally induced resistance changes

Figures 1(a) and 1(b) are plots of the percentage change in resistance $[\Delta R_{\text{mr0}}(t, T_{\text{mr}}) = 100\% \cdot [R_{\text{mr0}}(t, T_{\text{mr}}) R_{\rm mr0}(0,T_{\rm mr})]/R_{\rm mr0}(0,T_{\rm mr})$ as a function of joule-heating time (t) for AMR stripes that were heated by currents between 17.7 and 25.6 mA to temperatures $(T_{\rm mr})$ between 167°C and 424°C over a total time of 105 hours. The substrate temperature during joule heating is 70°C. The quantity $\Delta R_{\rm mr0}(t, T_{\rm mr})$ was measured at periodic intervals (at ambient temperature of around 21°C) when the joule heating was temporarily interrupted (see the section on thermal stress experiments). The AMR stripes all have a t_{mr} of 40.0 nm, a gap of 0.5 μ m, and a stripe height of 2.4 μ m. Given the electrical resistivity and relative thickness of the stripe layers, approximately 84% of the current flows through the Permalloy and 16% through the SAL. The current densities in the Permalloy are between 1.5×10^7 and 2.2×10^7 A cm⁻².

At temperatures below about 250°C [Figure 1(a)], the resistance is observed to decrease with joule-heating time (process 1). The time dependence of the resistance change for process 1 is best described by an exponential approach to a minimum resistance of $-\Delta R_1$ with a time constant τ_1 . As temperature increases, τ_1 decreases. At temperatures above ~300°C, the slope of the change in resistance becomes positive (process 2). The initial resistance increase follows a \sqrt{t} dependence. At a fixed temperature, for resistance increases above about 5%, the rate of resistance increase is slower than the initial \sqrt{t} dependence. For resistance increases up to about 8-10%, the resistance increase is fit well with a stretched exponential or Weibull function [18-22], which has a \sqrt{t} dependence in the exponential and approaches a maximum increase of ΔR , at long times. A stretched exponential time dependence was chosen because, in short times, it follows a \sqrt{t} dependence, which slows down with time. The data shown in Figures 1(a) and 1(b) has been fit using two processes, with the time dependence described

$$\Delta R_{\rm mr}(t, T_{\rm mr}) = -\Delta R_1 [1 - \exp(-(t/\tau_1))] + \Delta R_2 [1 - \exp(-\sqrt{t/\tau_2})]$$
(5a)

and the Arrhenius temperature dependence of $\tau_{\scriptscriptstyle 1}$ and $\tau_{\scriptscriptstyle 2}$ given by

$$\tau_i(T_{\rm mr}) = \tau_{0i} \exp(E_i/k_{\rm B}T_{\rm mr}) = 10^{S_i} \exp(E_i/k_{\rm B}T_{\rm mr}),$$
 (5b)

where the quantity $k_{\rm B}$ is the Boltzmann constant $(8.62\times 10^{-5}~{\rm eV}~{\rm cm}^{-1})$, $\tau_{0i}(=10^{S_i})$ is the prefactor, and E_i is the activation energy for the ith process. The data in Figures 1(a) and 1(b) is fit with $\Delta R_1=1.4\pm0.4\%$, $E_1=0.86\pm0.05~{\rm eV}$, $S_1=-7.0\pm0.5~{\rm log_{10}}({\rm hr})$, $\Delta R_2=9\pm1\%$, $E_2=2.1\pm0.1~{\rm eV}$, and $S_2=-14.2\pm0.5~{\rm log_{10}}({\rm hr})$. Resistance changes were also measured on parts with a $t_{\rm mr}$ of 30.0 nm and a gap of 0.37 μ m, and the same trends in resistance changes were observed, but with noticeably shorter values for τ_2 . While the activation energy for the resistance increase was the same for the 30.0-nm and the 40.0-nm parts, the prefactor for the 30.0-nm parts was ten times shorter than for the 40.0-nm parts. **Table 1** summarizes the thermodynamic parameters used to fit the observed resistance changes.

Amplitude changes from thermal stress

Figure 2 shows the percentage change in AMR amplitude at ± 120 Oe plotted against temperature for the same group of parts shown in Figures 1(a) and 1(b). Also included are the four elements used as controls, which were at the ambient substrate temperature of 70°C. Above about 175°C, the amplitude increases, reaching a maximum of 23 \pm 3% at around 275°C. For higher temperatures, the amplitude decreases, falling to its value

prior to heating, at around 425°C. These experiments were repeated on many other sensors with the same time dependence but with variations in the magnitude of the maximum amplitude increase of 30 \pm 15%. The time dependence of a change in amplitude normalized to the initial value of the sensors $[\Delta Amp(t,\,T_{\rm mr})=100\%[Amp(t)-Amp(t=0)]/Amp(t=0)]$ can be modeled using a stretched exponential for both the growth $[\Delta Amp_{\rm anneal}(t,\,T_{\rm mr})]$ and the decrease $[\Delta Amp_{\rm degrade}(t,\,T_{\rm mr})]$ in the amplitude using Equations (6b) and (6c), respectively:

$$\begin{split} \Delta Amp(t,\,T_{\rm mr}) &= \Delta Amp_{\rm anneal}(t,\,T_{\rm mr}) - \Delta Amp_{\rm degrade}(t,\,T_{\rm mr}); \\ &\qquad \qquad (6a) \\ \Delta Amp_{\rm anneal}(t,\,T_{\rm mr}) &= \Delta Amp_{a0}[1 - \exp(-\sqrt{t/\tau_{\rm a}(T_{\rm mr})})]; \\ \Delta Amp_{\rm degrade}(t,\,T_{\rm mr}) &= \Delta Amp_{d0}[1 - \exp(-\sqrt{t/\tau_{\rm d}(T_{\rm mr})})]. \end{split}$$

An Arrhenius temperature dependence [Equation (5b)] is used for both the annealing (τ_a) and the degradation (τ_d) time constants. ΔAmp_{a0} is the increase in AMR amplitude reached after the annealing process is completed, and ΔAmp_{d0} is the decrease in AMR amplitude associated with the degradation process. Further decreases in amplitude are expected for higher temperatures or longer times. The growth of the amplitude is fit with a value of 25 \pm 5% for ΔAmp_{s0} and Arrhenius parameters of $S_a = -15 \pm 0.5 \log_{10}(hr)$ and $E_a = 1.7 \pm 0.1$ eV (see Figure 2). Although the growth could also have been fit with an exponential having the same parameters used for the process 1 resistance decrease, the stretched exponential functional form was chosen to match with the time and temperature dependence of measured asymmetry changes (see Table 1),

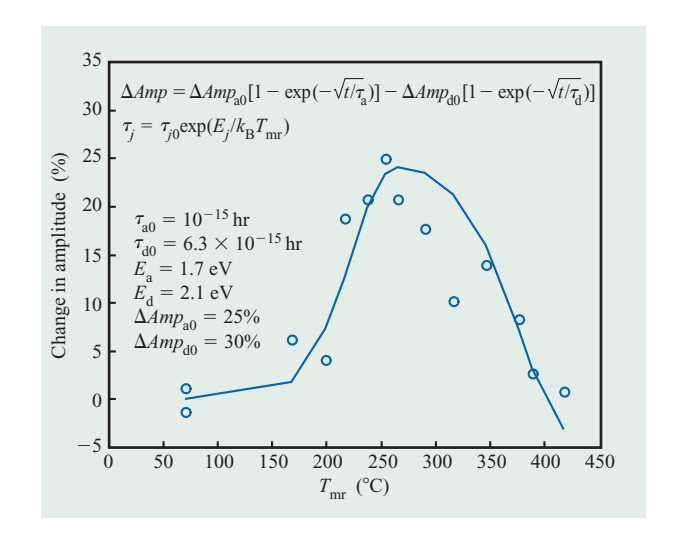


Figure 2

Change in AMR amplitude measured with a magnetic field of ± 120 Oe at $\sim 21^{\circ}$ C as a function of $T_{\rm mr}$ after 105 hours of joule heating. The fits are descibed in the text. The sensor $t_{\rm mr}$ and gap are 40.0 nm and 0.5 μ m, respectively.

which are described later. The fit to the degradation process (see **Figure 3**) uses a value of $30 \pm 5\%$ for ΔAmp_{d0} and the same Arrhenius parameters as used to fit the accompanying resistance increases: $S_{\rm d} = -14.2 \pm 0.5 \log_{10}({\rm hr})$ and $E_{\rm d} = 2.1 \pm 0.1 \ {\rm eV}.$

To better understand the annealing phenomenon, transfer curves of the AMR resistance plotted against magnetic field for fields up to ± 600 Oe were taken on parts with a $t_{\rm mr}$ value of 40.0 nm, a gap of 0.5 μ m, and an H of 2.5 μ m. Figure 3 plots the room-temperature

 Table 1
 Parameters used to fit the thermally induced changes in the electrical and magnetic properties of the AMR readers.

Process				$\log_{10}(au_{0i}) S_i$	Activation energy E_i	Potential mechanisms	
Parameter	Value (%)	Failure (%)	Fit type	$[\log_{10}(\mathrm{hr})]$	(eV)		
ΔR_1	1.5 ± 1.5	NA	Exp*	-7 ± 0.5	0.86 ± 0.1	Dislocation annealing or particle size growth	
$\Delta Amp_{_{\mathrm{a}0}}$	30 ± 15	NA	SE [†]	-15 ± 0.5	1.7 ± 0.1	Stress annealing or grain growth	
ΔAsy_{a0}	30 ± 15	20	SE^{\dagger}	-15 ± 0.5	1.7 ± 0.1	Stress annealing or grain growth	
$\Delta R_2 \ (t_{\rm mr} = 30 \ \rm nm)$	10 ± 1	6.5	SE^{\dagger}	-15.2 ± 0.5	2.1 ± 0.1	Interdiffusion, oxidation, electromigration	
$\Delta R_2 \ (t_{\rm mr} = 40 \ \rm nm)$	10 ± 1	6.5	SE^{\dagger}	-14.2 ± 0.5	2.1 ± 0.1	Interdiffusion, oxidation, electromigration	
$\Delta Amp_{d0}(t_{\rm mr} = 40 \text{ nm})$	30 ± 10	15	SE^{\dagger}	-14.2 ± 0.5	2.1 ± 0.1	Interdiffusion, oxidation, electromigration	

^{*}Exponential.

†Stretched exponential.

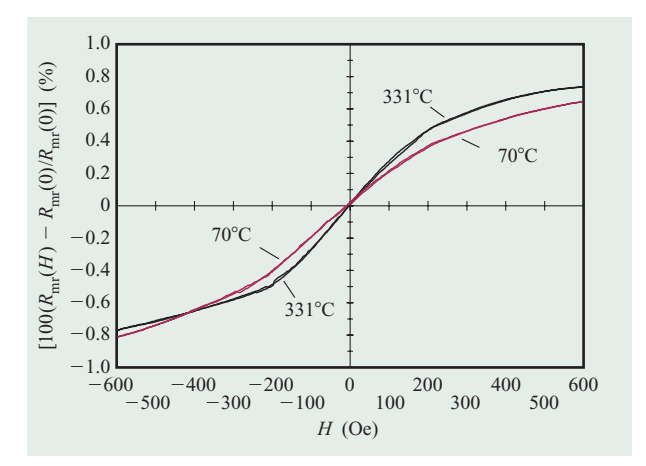


Figure 3

Normalized AMR amplitude plotted against a magnetic field measured at 21°C after 105 hours of joule heating at 70°C and 331°C. $T_{\rm mr}$ is 40.0 nm and gap is 0.50 μ m.

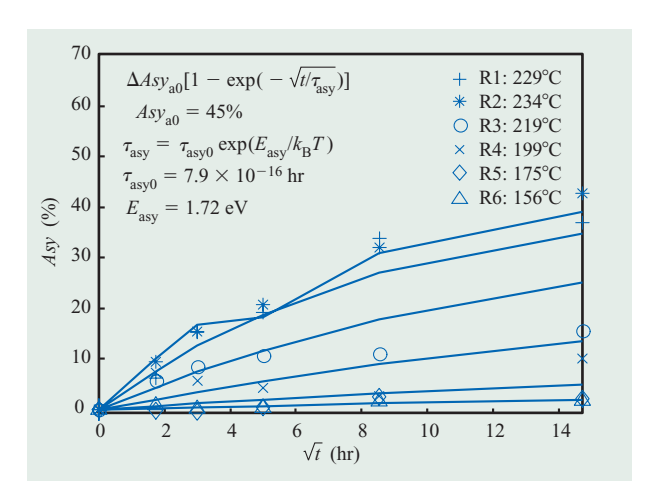


Figure 4

Change in asymmetry of AMR sensors measured with the quasistatic tester at a magnetic field of 0 and ± 120 Oe. The sensor $t_{\rm mr}$, gap, and H are 30.0 nm, 0.37 μ m, and 2.25 μ m, respectively. The fits are described in the text.

(~21°C) transfer curves for two sensors. One of the stripes was heated to 331°C for 105 hours via joule heating with a current of 24.6 mA (2.1×10^7 A cm⁻²). The second stripe was exposed for 105 hours to a minimal temperature of 70°C and no current. For fields of ± 600 Oe, the amplitude, as defined by Equation (4a), approached the saturation value of about 1.5%. The saturation amplitude remained at 1.5% after heating to 331°C, while the shape of the AMR transfer curves changed significantly. At

±120 Oe, the AMR amplitude increased from 0.46% of the zero field resistance for the stripe heated to only 70°C to 0.63% for the stripe heated to 331°C. Thus, the increase in AMR amplitude with annealing shown in Figure 2 is due to a change in the shape of the AMR signal as a function of field, not to an increase in the saturation level of the AMR signal at high fields.

Time dependence of thermally induced AMR asymmetry changes measured with a quasi-static magnetic field

Because improved amplitude is beneficial for drive reliability, and the degradation of the amplitude observed has such a large activation energy, attention was placed on measuring the time and temperature dependence of asymmetry changes associated with the observed annealing. To study the lower-temperature relaxation processes, sensors were heated to temperatures between 156°C and 234°C with currents between 17.3 and 21.3 mA for a duration of up to nine days. The stripe resistance and quasi-static AMR amplitude and asymmetry were measured at room temperature at intervals when the joule heating was interrupted. The sensors had a t_{mr} of 30.0 nm and an H of 2.3 μ m. The resistance changes followed the same behavior described earlier, but ΔR_1 was <0.1%, and the maximum resistance increase for the hottest sample was only 0.2%, as expected because of the relatively low temperatures. The amplitudes rose between 2% and 8%, but without a consistent trend. While the resistance and AMR amplitude changes were minor, the changes in AMR asymmetry were significant, with a maximum of +45% for the stripe with the highest $T_{\rm mr}$.

The time dependence of the change in quasi-static asymmetry relative to the initial values is shown in **Figure 4**. (The glitch in ΔAsy between nine and 25 hours for sensor R2 is the result of a temporary drop in $\Delta T_{\rm mr}$ for that stripe from a poor contact of the measurement probe during this one heating interval.) The asymmetry increased with time and temperature from 2% to 4% for sensors with $T_{\rm mr}$ values of 156°C and 175°C to 40 \pm 3% for sensors with $T_{\rm mr}$ values of 229°C and 234°C. The asymmetry increase is fit to a stretched exponential time dependence given by Equation (7a), with an Arrhenius temperature dependence for the time constant ΔAsy given by Equation (5b),

$$\Delta Asy_{\text{anneal}}(t, T_{\text{mr}}) = \Delta Asy_{\text{a0}} [1 - \exp(-\sqrt{t/\tau_{\text{Asy}}(T_{\text{mr}})})]. \tag{7}$$

In the case of sensor R2, $t/ au_{\rm Asy}(T_{\rm mr})$ in Equation (7) is replaced by $\int dt/ au_{\rm Asy}(T_{\rm mr}(t))$. The saturation asymmetry ($\Delta Asy_{\rm a0}$) used to fit the data is 45 \pm 5%. The Arrhenius parameters used for $au_{\rm Asy}$ are $S_{\rm Asy}=-15.1\pm0.7\,\log_{10}({\rm hr})$ and $E_{\rm Asy}=1.7\pm0.07\,{\rm eV}$ (see Table 1).

Time dependence of thermally induced AMR asymmetry changes measured with high-density magnetic transitions recorded on tape

Because the AMR response of a shielded sensor depends strongly on whether the applied field is homogeneous or of a high spatial density, for drive reliability analysis, it is important to measure the latter. A tape head with a $t_{measure}$ value of 30.0 nm, a gap of 0.37 μ m, and an H of 2.3 μ m is used to study the effect on the AMR asymmetry of exposure to elevated temperatures measured from transitions recorded on tape at 3.66×10^6 frpm. Six readers were heated for a maximum duration of 73 hours to between 172°C and 248°C via joule heating with currents from 20.1 mA to 22.7 mA. Two additional readers were at the substrate temperature of 40°C. Heating was interrupted at 3, 9, 25, and 73 hours, at which times five separate measurements of sensor asymmetry were taken at ambient room temperatures under normal $I_{\rm mr}$ values of 12 mA. The averages of each group of five tests were recorded. As is usual for the temperature region studied, the resistance changes were minimal. The magnetic amplitude changes ranged from +2% to +12%. Figure 5 is a plot of the asymmetry change as a function of \sqrt{t} . As with the quasi-static data, the time dependence of the asymmetry changes were fit with a stretched exponential given by Equation (7), with $\Delta Asy_{a0} = 20\%$. The Arrhenius parameters used for τ_{Asy} are $S_{\text{Asy}} = -14.8 \log_{10}(\text{hr})$ and $E_{\text{Asy}} = 1.7 \text{ eV}$, which are, within experimental error, the same as those used to fit the quasi-static data (Table 1).

Oxidation of the AMR stripe and the shields

Oxidation of the AMR stripe and of shields S1 and S2 was measured using an AFM for sensors that were exposed to elevated joule-heating temperatures. Figures 6(a), 6(b), and 6(c) are AFM line traces of the air-bearing surface of an AMR sensor following joule heating of the AMR stripe to 370°C with a current through the stripe of 23.2 mA for 100 hours. W, H, and gap are 12.6, 2.2, and 0.37 μ m, respectively. Figure 6(a) is a line trace perpendicular to the track width through the center of the stripe. The trace passes from right to left across a portion of the AlTiC substrate, the 3- μ m-thick undercoat alumina (UC), the 1.5-µm-thick Sendust shield S1, the AMR stripe, the 3.0-\mum-thick plated 81 Permallov shield S2, and 3 \mum of the overcoat alumina (OC) (see Figure 1 in [12], this issue). The gap alumina between shield S1 and the AMR stripe and between shield S2 and the AMR stripe is not resolved in this figure. In Figure 6(a), the height of shield S1 above the UC was essentially unchanged by the heating. The AMR stripe oxidized approximately 60 to 80 nm above its time-zero height. Shield S2 also oxidized substantially, with the oxidation being the highest on the edge closest to the AMR stripe and falling off with

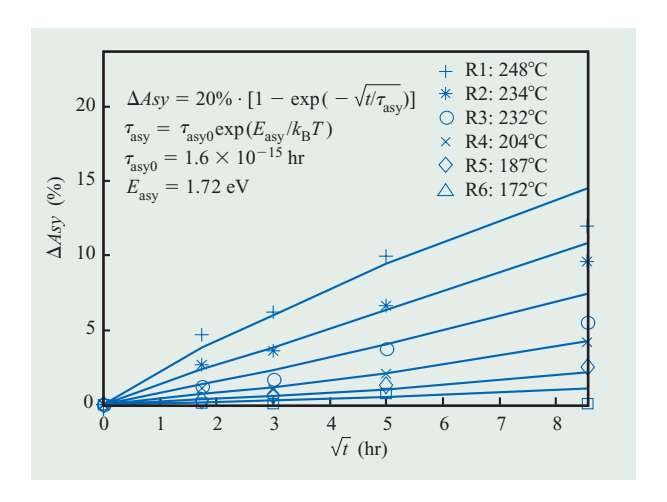


Figure 5

Time dependence of the change in asymmetry from tape signals measured at ~21°C as a function of \sqrt{t} . Heating temperatures are between 172°C and 248°C. The sensor $t_{\rm mr}$, gap, and H are 30.0 nm, 0.37 μ m, and 2.25 μ m, respectively. The fits are described in the text

distance along shield S2 away from the AMR stripe. Oxidation of the AMR stripe and of shield S2 can be distinguished by making a line trace along the direction parallel to the track width. Figure 6(b) is a line trace parallel to the track width along the AMR stripe. The oxidation is fairly uniform for the 12.6-µm length of the track width. The oxidation can be fit with a parabola centered on the AMR stripe and falling off weakly with distance along the track width. Beyond the width of the stripe, the oxidation falls abruptly because the leads are cool. Figure 6(c) is a line trace through shield S2 parallel to the track width and at a distance of 0.78 µm from the AMR stripe. The oxidation of shield S2 is fit by a Gaussian with an oxidation height of 23.3 nm and a Gaussian width of 5.0 μ m. The oxidation within shield S2 is easily determined by the temperature distribution within the shield [14, 23], with the hotter central portion having the most oxidation.

The peak oxidation height for the AMR stripe as a function of \sqrt{t} is shown in **Figure 7(a)** for times between 0.25 and 100 hours and AMR stripe temperatures between 248°C and 385°C. While the oxidation follows a dependence on \sqrt{t} for early times or lower oxidation heights $(x_{\rm ox})$, at higher oxidation heights and for longer times, the growth rate slows and approaches an asymptotic value. A stretched exponential function with a rate $k_{\rm ox}$ and an asymptotic height of x_0 fits the time dependence of the growth of the oxidation height of the AMR stripe:

$$x_{\text{ox}}(t, T) = x_0 [1 - \exp(-\sqrt{(k_{\text{ox}}t)})].$$
 (8a)

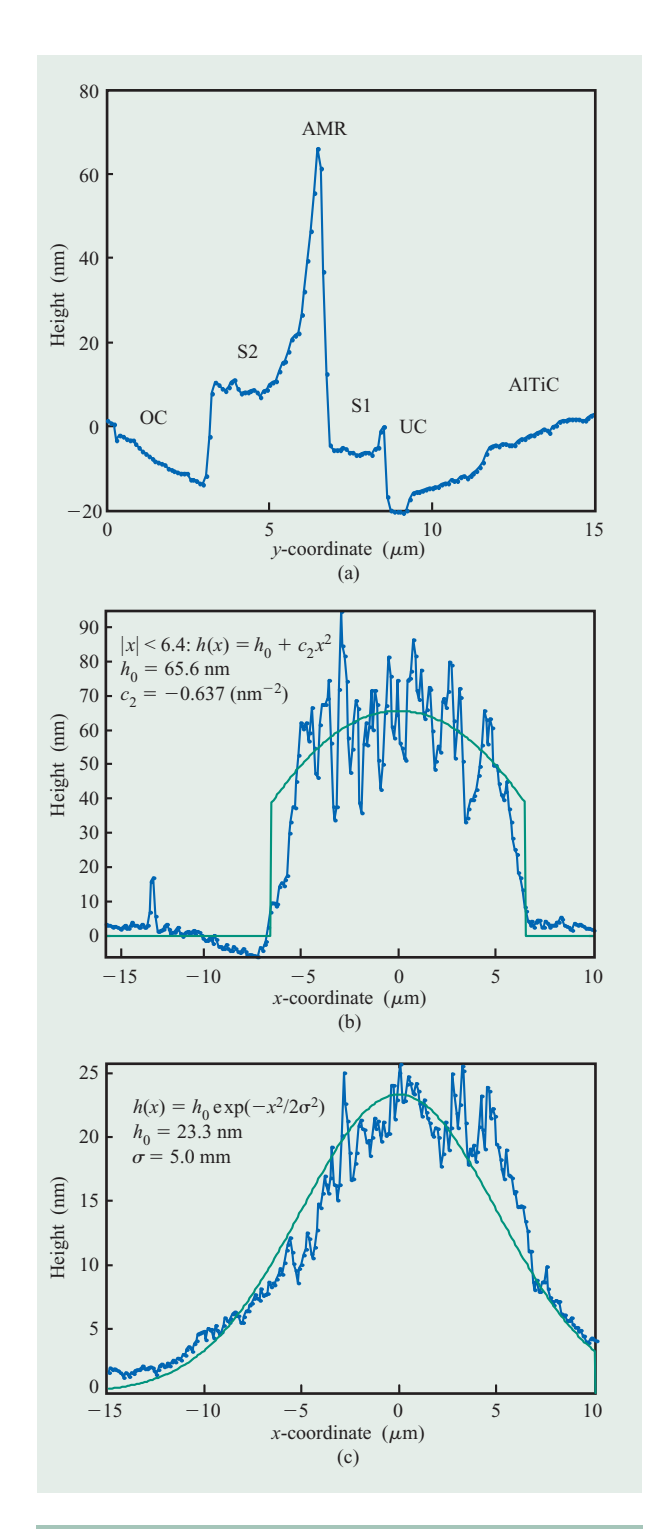


Figure 6

(a) AFM line traces of the air-bearing surface of an AMR sensor following 100 hours of joule heating of the AMR stripe to 370°C with a current of 23.2 mA. Line trace (a) is perpendicular to the track width through the AlTiC, UC, S1, MR, S2, and OC. Line trace (b) parallel to the track width along the stripe; (c) parallel to the track width 0.60 μ m into shield S2. W, H, and gap are 12.6, 2.2, and 0.37 μ m, respectively.

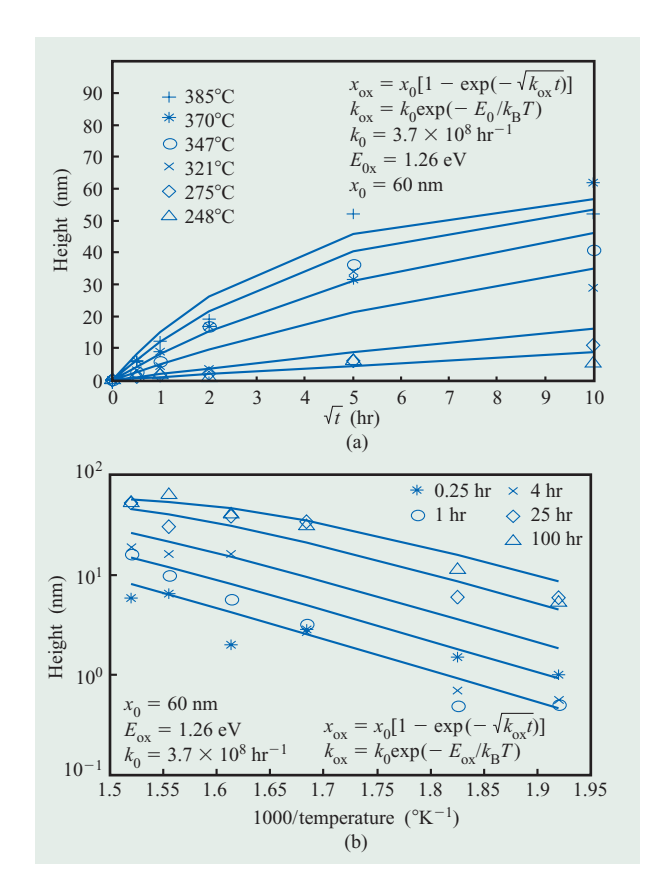


Figure 7

(a) Time dependence and (b) Arrhenius plot of the oxidation height at the center of the AMR stripe (x=0). The $t_{\rm mr}$ and gap are 30.0 nm and 0.37 μ m, respectively. The fits are described in the text.

The oxidation has an Arrhenius dependence on temperature [24], with a prefactor given by k_0 and an activation energy (E_{ox}) :

$$k_{ox} = k_0 \exp(-E_{ox}/k_B T). \tag{8b}$$

Arrhenius plots of the data using $T=T_{\rm mr}$ and fits to the height of the stripe oxidation at the fixed times of 0.25, 1, 4, 25, and 100 hours are shown in **Figure 7(b)**. For short times, when $k_{\rm ox}t\to 0$, the stretched exponential follows a \sqrt{t} dependence:

$$x_{ox}(t, T) = \sqrt{(k_0 x_0^2 t)} = \sqrt{Dt},$$
 (9a)

with

$$D = k_0 x_0^2 \exp(-E_{ox}/k_B T) = D_0 \exp(-E_{ox}/k_B T).$$
 (9b)

Equation (9a) represents a standard diffusion process with a diffusion coefficient (D) given by Equation (8b). $D_{\scriptscriptstyle 0}$ and $E_{\scriptscriptstyle {\rm ox}}$ respectively are the prefactor and the activation energy

of the diffusion process. The growth of the oxidation height for the AMR stripe is fit using Equations (8a) and (8b), with $x_0 = 59$ nm, $k_0 = 4 \times 10^8$ hr⁻¹, and $E_{\rm ox} = 1.26$ eV (**Table 2**). The diffusion prefactor for the stripe (D_0) can be determined for oxidation levels below about 30 nm using Equation (9b), which yields a value of $D_0 = 1.3 \times 10^{12}$ nm² hr⁻¹.

The growth of the oxidation height of shield S2 is substantially smaller than that of the MR stripe and is essentially linear in \sqrt{t} . Because of the lower oxidation growth on shield S2, a wider range of temperatures on more parts was acquired in order to achieve a sufficient signal-to-noise ratio. **Figure 8** is an Arrhenius plot of the peak S2 oxidation height at a fixed time of 56 hours for a group of 12 sensors with AMR stripe temperatures of between 211°C and 383°C. The data is fit using Equations (9a) and (9b), with the temperature being given by the shield S2 temperature at the measurement location (T_{c2}) :

$$T_{s2} = T_s + f_{s2}(T_{mr} - T_s),$$
 (10)

with $f_{\rm s2}=0.75$. Equation (10) assumes that at a fixed location on shield S2, the temperature rise due to joule heating above the substrate temperature is proportional to the AMR temperature rise. Finite element analysis (FEA) confirms this and yields values of $f_{\rm s2}$ of 0.75 ± 0.1 , depending on the thermal conductivities chosen [14, 23]. Fits to the data (Figure 8) yield a diffusion prefactor of $D_0=10^{12\pm0.6}~{\rm hr}^{-1}$ and an activation energy $E_{\rm ox}=1.24\pm0.07~{\rm eV}$, which, within the accuracy of the data, are the same as the values measured for oxidation of the AMR stripe.

Wallace-spacing losses

One effect of oxidation is to degrade signal amplitude as a function of the longitudinal density of magnetic transitions written on the tape. This magnetic density-dependent response, termed Wallace-spacing losses [4, 10], is described by

$$Amp(d, \lambda) = Amp_0 \exp(-2\pi d/\lambda), \tag{11}$$

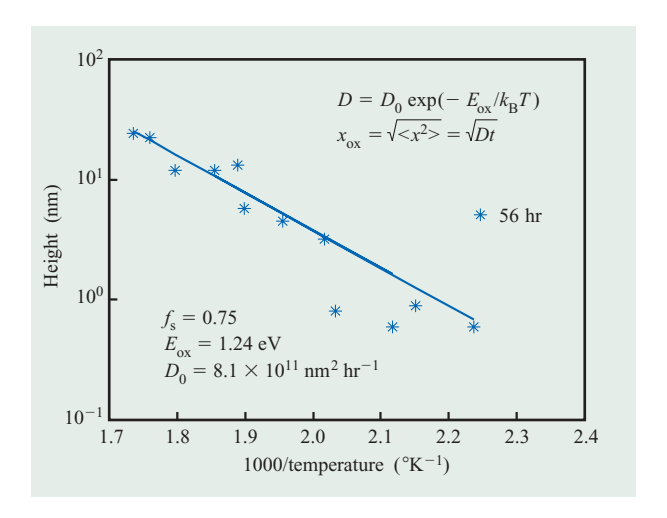


Figure 8

Arrhenius plot of the oxidation height on shield S2 at the edge closest to the gap (y-axis) and centered with respect to the AMR stripe (x = 0). The $t_{\rm mr}$ and gap are 30.0 nm and 0.37 μ m, respectively. The fits are described in the text.

where d is the spacing between the magnetic coating on the tape and the sensor ABS, λ is the wavelength of the pattern written on tape, and Amp_0 is the amplitude at d = 0. The wavelengths used in a drive depend on the channel code [11, 25]. For the code used in this study, the shortest wavelength ($\lambda_{short} = 546 \text{ nm}$) is twice the inverse of the highest transition density. The longest wavelength $(\lambda_{long} = 2186 \text{ nm})$ is four times λ_{short} . For an oxidation height of 40 nm, signal amplitudes from data written with wavelengths of λ_{short} and λ_{long} would be decreased respectively to 63% and 89% of their values prior to oxidation. Although modern tape drives have dynamic automated amplifiers to compensate for signal losses, compensation for the change in read pulse shape requires the development and implementation of complicated dynamic automated algorithms that have frequency-dependent amplification. The combination of the loss in amplitude and the change in pulse shape can result in a significant decrease in the BER. As drives

Table 2 Parameters used to fit the oxidation of the AMR stripe and shield S2.

Process		Failure	x_0	E_{ox}	Sox	$log_{10}(D_0)$
Location	Fit type	<i>height</i> (nm)	(nm)	(eV)	$[\log_{10}(k_{\rm ox})]$	$[\log_{10}(\mathrm{hr})]$
MR stripe Shield S2	SE* Diff [†]	40 40	59 ± 10 NA	1.26 ± 0.1 1.24 ± 0.1	8.6 ± 0.5 NA	$12.1 \pm 0.7^{\ddagger} 12.0 \pm 0.5$

^{*}Stretched exponential.

[†]Diffusion

[‡]Calculated using Equation (9b).

evolve, the effect of Wallace spacing will become more significant. For example, if the linear density increases by a factor of 3, the amplitudes from $\lambda_{\rm short}$ and $\lambda_{\rm long}$ will drop respectively to 25% and 71% of the zero-spacing losses. It will be difficult to compensate for such large decreases in signal amplitude combined with the dramatic distortion of the signal shapes. Thus, tolerances on oxidation levels must be tighter for future-generation drives.

Mechanisms for the observed electrical and magnetic changes

Oxidation

One contributor to the resistance increase ΔR_2 and associated drop in AMR amplitude is oxidation. The 1.25 ± 0.15 eV activation energy measured for stripe oxidation at the ABS matches the value of 1.2 \pm 0.4 eV measured on Permalloy sheets exposed to air [9]. The oxidation measured in this report is projected to be ~11 nm after 200 hours at 250°C, which is similar to the amount of oxidation recorded by Bajorek and Mayadas [9] on thin films of Permalloy. In their experiments, the effect of oxidation over a 200-hour period at 250°C was significant for 20.0-nm-thick sheets and reduced by a factor of ~3 for 40.0-nm-thick sheets, yielding an oxidation height of ~16 nm. The large magnetic changes observed by Bajorek and Mayadas were a result of substantial oxidation relative to the sheet thickness. For the functional readers studied in this report, the sheet surface area is protected by alumina, and only material at the ABS is exposed to air. The fractional loss in amplitude from oxidation at the ABS is given by the ratio of the oxidation height to the stripe height (x_{ox}/H) , which is only 0.5% for 11-nm oxidation of a stripe with an H of 2 μ m. Even at the highest temperatures and longest times in this study, the oxidation accounted for a resistance change of only about 2-3%, while the total resistance increase was 9% and the AMR amplitude degradation was 20-40%. Furthermore, the large resistance increases can be described by an activation energy of 2.1 eV, which is 70% greater than the activation energy for oxidation. Thus, additional mechanisms must be present to completely account for ΔR_2 .

Interdiffusion

Another mechanism that could increase resistance is interdiffusion of the metals between the multilayered stripe. Simple diffusion models predict that the time for the resistance to increase by a fixed fractional amount ($\tau_{\rm ID}$) should be proportional to the square of the stripe thickness: $\tau_{\rm ID} \sim t_{\rm mr}^2$. When changing from a 30.0- to a 40.0-nm-thick stripe, $\tau_{\rm ID}$ should increase by a factor of

only 1.8, while τ_2 is measured to increase by a factor of 10. Thus, in addition to oxidation and interdiffusion, a third mechanism must be invoked to explain the bulk of ΔR_2 .

Electromigration

The measured activation energy of 2.1 ± 0.1 eV for the large resistance increases and the amplitude degradation for the sensors with $t_{\rm mr}$ values of 30.0 and 40.0 nm match the value of 2.0 ± 0.1 eV measured on 20.0-nm-thick dual-stripe AMR sensors [6] and the 2.2 \pm 0.5 eV for magnetic changes on 21.0-nm-thick Permalloy stripes [9]. Furthermore, the increase in the rate prefactor measured in this study (to $6.3 \times 10^{-16} \text{ hr}^{-1} \text{ from } 6.3 \times 10^{-15} \text{ hr}^{-1}$ for the sensors with a $t_{\rm mr}$ of 30.0 nm compared with the sensors with a $t_{\rm mr}$ of 40.0 nm) correlates with a rate prefactor of 10^{-16} hr⁻¹ measured by Zolla [6] for a 20.0-nm-thick stripe. In Zolla's experiments, the large resistance increase was ascribed to either "electromigration-induced segregation of the Fe followed by oxidation or preferential oxidation of Fe." Direct observation of electromigration-induced microsegregation of the Ni and Fe atoms was made in the studies by Moore, Turner, and Tai [7] on unannealed 100.0-nmthick film of Permallov using current levels of 0.5×10^6 to $0.7 \times 10^6 \, \text{A cm}^{-2}$.

Besides the data of Moore, Turner, and Tai, the large increase in process 2 rates on going from a stripe thickness of 40.0 to 20.0 nm supports the possibility of electromigration. Studies on electromigration indicate that the time-to-failure for an electromigration process ($\tau_{\rm EM}$) can be described [8, 26] by

$$\tau_{\rm EM} = AJ^{-n} \exp(\Delta H/k_{\rm B}T_{\rm mr}),\tag{12}$$

where A is a constant, J is the current density, and ΔH is the activated energy of the diffusion process. Values of n usually range from 2 to 3. For the ranges of J used to measure the effects of thermal stress on an AMR stripe of a fixed thickness, the temperature variations and scatter in the data overshadow the contribution from the J^{-n} factor of the electromigration effect. For the data shown in Figure 1(b) with n = 3, the J^{-n} term changes τ_{EM} by a factor of only \sim 3 for *n* and the current range of 17.7 to 25.6 mA, while the activation energy of 2.1 eV results in a factor of ${\sim}3000$ increase in $\tau_{\rm EM}$ for the temperature range of 295°C to 424°C. Furthermore, on an Arrhenius plot covering several decades in time, a pure Arrhenius temperature dependence [Equation (5b)] and an electromigration process [Equation (12)] are indistinguishable. However, a comparison of experiments on sensors designed with large differences in t_{mr} , gap, H, and W can reveal electromigration effects because the current density results in a fixed temperature [12]. To

achieve a fixed temperature, current densities are substantially different for different geometries. In Zolla's experiments, the currents used were between 10.5 and 12.5 mA for temperatures between 250°C and 400°C. Assuming that H was $\sim 1 \mu m$, the current densities were 5×10^7 and 6×10^7 A cm⁻². For the experiments in this study, the current densities needed to achieve a temperature rise of 390°C were respectively about 2.3×10^7 and 3×10^7 A cm⁻² for the 40.0- and 30.0-nm-thick sensors. Using Equation (10) to describe τ_2 for the 20-, 30-, and 40-nmthick sensors yields a value of \sim 4.5 for n with only a minor decrease in the activation energy. Thus, electromigration contributes substantially to the measured resistance increases. Since interdiffusion rates also increase with a decrease in stripe thickness, 4.5 is an upper limit for n. An accurate determination of n and of the contribution of interdiffusion and oxidation requires the data to be fit using Equation (10) for τ_2 , and the introduction of additional processes for interdiffusion and oxidation into Equation (5). Because the data for a fixed sensor geometry is fit well with only a single process for ΔR_2 , separation of electromigration, oxidation, and interdiffusion is difficult and would require data from a wide range of both sensor geometries (specifically H and t_{mr}) and current densities to properly decouple the different processes. A combination of oven and joule heating to achieve the desired temperatures can also help determine the contributions from electromigration. The fact that ΔR_2 can be fit well with a single activation energy can be justified by the fact that the same materials involved in interdiffusion are also involved in electromigration, and that oxidation is not the major contributor to the resistance increases. With the decreases in $t_{\rm mr}$ for future-generation products, the rates for both electromigration and interdiffusion will increase.

Annealing

An important question is what causes the lowertemperature (≤250°C) resistance, asymmetry, and amplitude changes observed in the experiments reported here. Despite the overlap in times and temperatures for the observation of the resistance drop ΔR_1 and the lowtemperature increase in the AMR amplitude and asymmetry, the causes of these changes are probably different because they have such different time profiles and activation energies. The activation energy for the resistance drop (0.86 \pm 0.1 eV) is close to the values measured for electromigration (0.7 \pm 0.1 eV) [8], for the diffusive processes of particle size growth $(0.7 \pm 0.05 \text{ eV})$ [27], and for dislocation annealing (0.7 eV) [28]. Because the electromigration phenomenon measured by Gangulee and d'Heurle [8] resulted in catastrophic failure, it is clearly not the mechanism

involved in ΔR_1 . Furthermore, the low-activation-energy electromigration phenomenon measured by Gangulee and d'Heurle was essentially eliminated by annealing the samples prior to use, which is the standard processing practice for extant sensors. The most likely cause of ΔR_1 is particle size growth or dislocation annealing that results in an improved conductivity of the alloy, and thus a lower overall resistance.

One possible mechanism for the changes in the sensor magnetic properties is grain growth. The activation energy $(1.86 \pm 0.15 \text{ eV})$ and prefactor $(2.3 \times 10^{-15} \text{ hr})$ measured for grain growth [27] match the values measured for ΔAmp_{a0} and ΔAsy_{a0} in this paper (Table 1). Another possible explanation of the changes in AMR transfer curves observed following joule heating to between 200°C and 275°C is the annealing of stresses on the AMR sensor [29]. For magnetic materials that have a nonzero magnetostriction, stress can affect the magnetization transfer curve [1] which, in turn, can affect the AMR transfer curve. Although the Curie temperatures of the materials are all substantially higher than the operating temperatures, changes in the magnetic properties of magnetic materials due to annealing have been observed considerably below the Curie temperatures [1, 9, 29, 30]. Magnetic changes ascribed to stress relief on materials with nonzero magnetostriction have been observed in materials annealed at temperatures as low as 100°C [30]. In forming AMR sensors, the magnetic materials are deposited on a wafer as thin sheets by a sputtering ionbeam deposition or by a plating process. To achieve the desired magnetic properties, the magnetic materials are deposited at elevated temperatures [5] or are annealed at elevated temperatures subsequent to deposition. Because the magnetic materials have thermal expansion coefficients different from those of the materials surrounding them, they will be under stress from the heating and cooling cycles during processing [30] and operation [5, 15, 31]. Furthermore, the cutting and polishing of the wafer required to make a functional device can induce stresses in the magnetic materials. Stress, in turn, can affect the magnetic properties of the stripe through magnetostriction [13, 14].

Extrapolated time-to-failure

Several different processes have been discussed in this paper, including stripe resistance decreases (ΔR_1) and increases (ΔR_2) , amplitude decreases $(-\Delta Amp_{\text{degrade}})$ and increases $(\Delta Amp_{\text{anneal}})$, asymmetry increases $(\Delta Asy_{\text{anneal}})$, and the oxidation of the AMR stripe and shield S2. Tables 1 and 2 summarize the thermodynamic parameters used to fit the changes for the different processes as well as the magnitudes of the effects. The TTF for a given process can be determined by solving for the time to

425

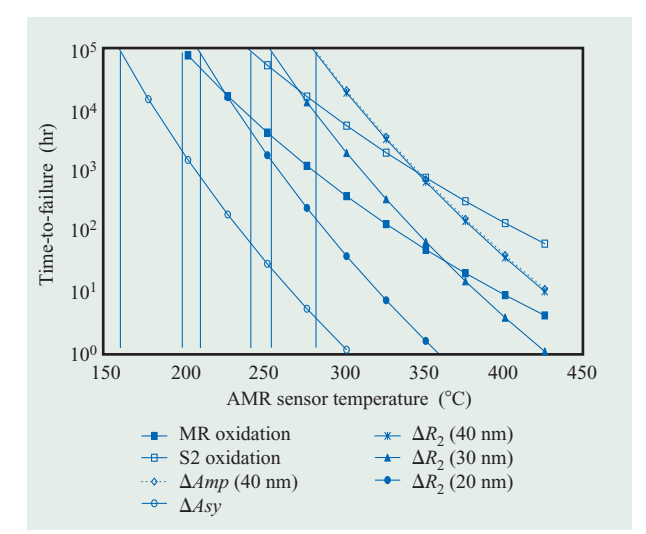


Figure 9

Projected TTF plotted against sensor temperature for amplitude degradation, asymmetry changes, resistance changes, and oxidation of the AMR stripe or shield S2. The TTF for ΔR_2 for sensors with a $t_{\rm rec}$ of 20.0 nm is taken from the report by Zolla [6].

reach a failure value using the appropriate equation. For asymmetry changes, Equation (7) can be used to determine the time $[TTF_{\rm Asymmetry}(T_{\rm mr})]$ for the sensor asymmetry to reach a value beyond which the drive will fail $(\Delta Asy_{\rm fail})$:

$$TTF_{\text{Asymmetry}}(T_{\text{mr}}) = \left[\log_{e}(1 - \Delta Asy_{\text{fail}}/\Delta Asy_{\text{a0}})\right]^{2} \tau_{\text{Asy}}(T_{\text{mr}}). \tag{13}$$

Similar equations can be constructed for the other quantities measured. Figure 9 is a plot of TTF for the amplitude degradation, asymmetry annealing, and oxidation of the AMR stripe and of shield S2 using the parameters given in Tables 1 and 2. Also shown in Figure 9 is the projected TTF for resistance changes of ~4% to 6% for the dual-stripe AMR sensor with a t_{mr} of 20.0 nm. In Table 1, the choice of 6.5% for $\Delta R_{\rm 2~fail}$ is used to correlate with $\Delta Amp_{\text{degrade fail}}$ of 15% and the failure point of Zolla [6] for large resistance changes on parts with t_{mr} values of 20.0 nm. Though the J^{-n} factor for electromigration [Equation (12)] was not explicitly included in the calculation of the TTF, analysis shows that for a fixed geometry, the Arrhenius [Equation (5b)] and the electromigration equations are indistinguishable, with only a minor difference in the activation energy used. The effect of electromigration on the large resistance increases, though, is clear in the dramatic decrease of TTF for t_{mr} (decreasing from 40.0 nm to 20.0 nm).

Conclusion

The data and analysis presented in this paper show that it is necessary to perform time- and temperature-dependent measurements on a variety of parameters to determine the thermal reliability of an AMR sensor for extended times and normal drive conditions. Though resistance is a relatively easy parameter to measure, it is difficult to extract the effects on the parameters relevant for accurate drive reliability projections. The elevated thermal stress tests reported here yield continuous changes in the measured parameters with both time and temperature, indicating that the materials are not experiencing any phase transitions within the temperature ranges used in the study. Thus, the thermodynamic parameters determined by the measurements and fits to the data should yield accurate projections of sensor reliability for extended use under normal operating conditions.

It has also been shown that a combination of stripe oxidation, electromigration, and interdiffusion is responsible for resistance increases and the concomitant degradation of the AMR amplitude. For the devices studied, electromigration and interdiffusion are not factors that affect the reliability of an AMR sensor for stripe temperatures below 250°C and for up to ten years of operation for extant drives. With future generations of tape drives, decreases in the stripe thickness will substantially decrease the TTF as a result of both electromigration and interdiffusion, requiring appropriate limitations in the current densities and stripe temperatures. The data shows that for extant drives, the only two quantities related to drive reliability that undergo changes for AMR stripe temperatures below 200°C are the AMR stripe oxidation and the increase in asymmetry due to annealing. Extrapolation of the TTF indicates that, for a product life of ten years, asymmetry changes due to annealing become problematic for the devices studied only for temperatures above about 160°C and oxidation effects for temperatures above about 190°C. One possible explanation for the low-temperature magnetic changes is stress relief annealing. Because stresses that develop during mechanical processing of the device cannot be eliminated by standard annealing during wafer processing, product sensors must be routinely monitored to ensure adequate reliability. While thermally accelerated stripe oxidation is not problematic for extant drives, increases in the longitudinal density of stored data written on tape with future-generation products will result in a decrease in the TTF associated with stripe and shield oxidation through Wallace-spacing losses, requiring tighter tolerances in the allowed oxidation heights. As evidenced by the lack of oxidation of the Sendust shield S1 compared with the Permalloy shield S2, different shield materials oxidize at different rates. Thus, resistance to thermal oxidation must be included in the parameters of

426

interest when selecting a new shield material for other purposes, such as wear resistance or increased magnetic permeability [31].

Acknowledgment

The author thanks the IBM Tape Head Development Group managed by Gary Decad for fabricating the parts used in this work, with special thanks to Darrell Follett for performing the magnetic measurements, to Peter Koeppe for reading the manuscript and giving useful comments, to Leif Kirshenbaum for discussions about magnetic characteristics and for maintaining the quasistatic magnetic tester, and to Yu-Min Lee, Benjamin Haskel, David Braunstein, Cheryl Liang, and Jason Liang for performing AFM measurements. The author also thanks Michael Ho of the IBM Almaden Research Center for lending the use of his quasi-static magnetic tester, and Peter Melz, who at the time was with the IBM HDD Reliability Group, for his many discussions on the reliability of AMR sensors.

References

- 1. R. M. Bozorth, *Ferromagnetism*, IEEE Press, Piscataway, NJ, 1951.
- R. P. Hunt, "A Magnetoresistive Readout Transducer," IEEE Trans. Magn. 7, No. 1, 150-154 (March 1971).
- J. C. Mallinson, The Foundations of Magnetic Recording, Second Edition, Mallinson Magnetics, Inc., Carlsbad, CA, 1987
- H. N. Bertram, Theory of Magnetic Recording, Cambridge University Press, Cambridge, England, 1994.
- R. H. Dee and R. F. M. Thornly, "Thermal Effects in Shield MR Heads for Tape Applications," *IEEE Trans.* Magn. 27, No. 6, 4704–4706 (June 1991).
- H. G. Zolla, "Thermal and Electrical Reliability of Dual-Stripe MR Heads," *IEEE Trans. Magn.* 33, No. 5, 2914– 2916 (September 1997).
- G. E. Moore, P. A. Turner, and K. L. Tai, "Current Density Limitations in Permalloy Magnetic Detectors," AIP Conf. Proc. 10, 217–221 (1972).
- 8. A. Gangulee and F. M. D'Heurle, "Electromigration and Diffusion in Ni–Fe Thin Films," *Jpn. J. Appl. Phys. Suppl.* **2**, 625–627 (1974).
- C. H. Bajorek and A. F. Mayadas, "Reliability of Magnetoresistive Bubble Sensors," AIP Conf. Proc. 10, 212–216 (1972).
- R. L. Wallace, Jr., "The Reproduction of Magnetically Recorded Signals," *Bell Syst. Tech. J.* 30, 1145–1173 (October 1951).
- 11. A. Taratorin, PRML: A Practical Approach, Introduction of PRML Concepts and Measurements, Guzik Technology Enterprises, Inc., Mountain View, CA, 1995.
- 12. I. E. T. Iben, Y.-M. Lee, and W. D. Hsiao, "Steady-State Thermal Characteristics of AMR Read/Write Heads Used in Tape Storage Drives," *IBM J. Res. & Dev.* 47, No. 4, 401–414 (this issue, 2003).
- R. M. Bozorth and H. J. Williams, "Effect of Small Stresses on Magnetic Properties," Rev. Mod. Phys. 17, No. 1, 72–80 (1945).
- O. E. Buckley and L. W. McKeehan, "Effect of Tension upon Magnetization and Magnetic Hysteresis in Permalloy," *Magnetization & Magn. Hysteresis* 26, 261–273 (1925).

- 15. K. F. Young, "Finite Element Analysis of Planar Stress Anisotropy and Thermal Behavior in Thin Films," *IBM J. Res. & Dev.* **34**, No. 5, 706–717 (1990).
- A. Oates, "Thin-Film Electromigration: Al Alloy Metallizations for Submicron IC Technologies," Proceedings of the IEEE International Reliability Physics Symposium, 1994, Tutorial Notes, pp. 2.1–2.23.
- J. W. McPherson, "Reliability/Processing Challenges for ULSI Metallization," *Proceedings of the IEEE International Reliability Physics Symposium*, 1994, Tutorial Notes, pp. 8.1–8.48.
- 18. W. Weibull, "A Statistical Distribution Function of Wide Applicability," *J. Appl. Mech.* **18**, 293–297 (1951).
- P. Tobias and D. Trindade, Applied Reliability, Van Nostrand, New York, 1995.
- 20. S. A. Brawer, *Relaxation in Viscous Liquids and Glasses*, American Ceramic Society, Columbus, OH, 1985.
- R. Zallen, The Physics of Amorphous Solids, John Wiley & Sons, Inc., New York, 1983.
- 22. I. E. T. Iben, D. Braunstein, W. Doster, H. Frauenfelder, M. K. Hong, J. B. Johnson, S. Luck, P. Ormos, A. Schulte, P. J. Steinbach, A. H. Xie, and R. D. Young, "Glassy Behavior of a Protein," *Phys. Rev. Lett.* 62, No. 16, 1916–1919 (1989).
- 23. Y. S. Ju, R. Xu, X. Wu, N. Smith, R. Fontana, W. Lee, K. Carey, M. Ho, D. Hsiao, and B. Gurney, "A Combined Experimental and Numerical Study of Temperature Rise in GMR Sensors Due to Self-Heating," *IEEE Trans. Magn.* 37, No. 4, 1701–1703 (2001).
- 24. C. Kittel, *Introduction to Solid State Physics*, Fifth Edition, John Wiley & Sons, Inc., New York, 1976, pp. 542–545.
- C. D. Mee and E. D. Daniel, Eds., Magnetic Storage Handbook, Second Edition, McGraw-Hill, Inc., New York, 1990.
- J. R. Black, "Electromigration—Brief Survey and Some Recent Results," *IEEE Trans. Electron Devices* 16, 338–347 (1969).
- 27. S. Krongelb, A. Gangulee, and G. Das, "Annealing of Thin Magnetoresistive Permalloy Films," *IEEE Trans. Magn.* **9**, No. 3, 568–570 (September 1973).
- 28. A. Gangulee and R. L. Anderson, "Annealing Behavior of Electroplated Permalloy Thick Films, II," *J. Electron. Mater.* 3, 171–187 (1974).
- R. M. Bozorth and J. F. Dillinger, "Heat Treatment of Magnetic Materials in a Magnetic Field. II. Experiments with Alloys," *Physics* 6, 285–291 (1935).
- J. H. Howey, "Magnetic Behavior of Nickel and Iron Films Condensed in a Vacuum upon Various Metal Backings," *Physiol. Rev.* 34, 1440–1447 (1929).
- 31. M. Jursich, K. Rook, M. Henderson, and D. Liu, "Alternate Pole Materials for MR Tape Heads," *IEEE Trans. Magn.* **32**, No. 1, 156–159 (January 1996).

Received September 13, 2002; accepted for publication January 20, 2003

Icko Eric Timothy Iben IBM Tape Head Development Group, 5600 Cottle Road, San Jose, California 95193 (iben@us.ibm.com). Dr. Iben is a Senior Engineer in the Tape Head Development group. He received his B.S. degree in physics from the University of California at Berkeley in 1980 and his Ph.D. degree in physics from the University of Illinois in 1988. Prior to joining IBM, Dr. Iben worked for three years at AT&T Bell Laboratories and New York University doing biophysics research. He then worked for General Electric Research and Development in the areas of environmental remediation, medical instrumentation, and material characterization. He has been with IBM since 1997, performing reliability testing for tape heads.